Construction and Characterization of a Quantum Diamond Microscope

A Major Qualifying Project submitted in partial completion of graduation requirements by

Federico Poggioli

Advisors: Professors Raisa Trubko and Douglas Petkie

WPI

Worcester Polytechnic Institute
Worcester, MA, USA
May 10, 2021

Abstract

The Quantum Diamond Microscope (QDM) is a novel instrument that utilizes Nitrogen-vacancy centers in diamond to image magnetic fields via Optically Detected Magnetic Resonance (ODMR) spectroscopy. A QDM is constructed and a study of its components and principles of operation is carried out. The effects of varying laser power, microwave power, and bias magnetic field on the ODMR spectrum are studied experimentally. From these studies, optimal experimental parameters for taking magnetic field measurements with this QDM were determined to be at least 3W of laser power and -15dBm of microwave power. The effect of data collection time on the measured background noise was also studied. This QDM reached less than $1\mu T$ of background noise after 2 hours and $0.5\mu T$ of background noise after 8 hours. Finally, the magnetic field of a solenoid was successfully measured as a demonstration of the QDM.

Acknowledgements

First and foremost, I would like to thank my advisors, Professors Douglas Petkie and Raisa Trubko, for their support during the development of this project. I am particularly thankful for the mentorship and guidance Professor Trubko gave me.

Work on this MQP project was never done alone. For this reason, I would also like to thank the other members of the WPI Trubko Group for being there to help out. They are Camille McDonnell, William Aaron, Amelia Nishimura and Daniil Volkov.

One of the important parts of the work carried out on this report would not have been possible without the initiative of Thomas Lipkin and his MQP group, who lend us the solenoid actuator that was used for the solenoid measurements.

Contents

List of Figures

List of Tables

Chapter 1

Introduction and Objectives

1.1 The Quantum Diamond Microscope

Beginning in the 1950's, long after the foundations of Quantum Mechanics were well established, scientists and engineers began to utilize the principles of quantum mechanics to construct devices that enable our modern technology. Transistors, lasers, MRI machines and Scanning Tunneling Microscopes are a few examples of revolutionary devices whose principles of operation are grounded in Quantum Theory. The Quantum Diamond Microscope (QDM) is among the most recent additions to this list [**7**]. The QDM uses a diamond crystal that contains Nitrogen-vacancy (NV) defects on its lattice. The unique features of the energy level structure of these NV centers makes them useful for sensing magnetic fields. The QDM uses Optically Detected Magnetic Resonance (ODMR) spectroscopy to measure magnetic fields with micrometer-scale spatial resolution.

The QDM is a promising device for magnetic field measurements due to its unique capabilities. It offers broader fields of view and better DC resolution than Magnetic Force Microscopy (MFM), as well as higher spatial resolution than a superconducting quantum interference device (SQUID) [**2**]. QDM measurements can be carried out at room temperature, and do not require the use of specialized components besides the NV diamond itself. These properties make the QDM a useful device for imaging applications in different fields. It has been used to measure current flow in graphene, to determine the position of magnetically labeled cells, and to study the magnetic field of geological samples from both Earth and outer space, and more [**1**, **5**, **7**].

The QDM has several key components (shown in Fig. 1.1): a 532nm laser for exciting the NV system, an array of Helmholtz coils or permanent magnets for generating a bias magnetic field, a RF circuit for generating a microwave field, and a high-resolution camera and microscope objective for imaging. The laser is used to excite the NV centers, which can then emit red fluorescence when they decay back to the ground state. The fluorescence is imaged by a camera. The amount of fluorescence that is emitted depends on the ground state spins of the NV centers' electrons. Importantly, the spin can also be controlled using resonant microwaves. In order to conduct a magnetic field measurement, the sample of interest is placed near the NV diamond. The magnetic field from the sample results in a Zeeman shift to the NV energy levels and changes the microwave resonance frequencies, which in turn produce changes in the amount of fluorescence detected at a given microwave frequency. By measuring changes in fluorescence as a function of

microwave frequency, it is possible to determine the shift of resonance frequencies and therefore the magnetic field of the sample. Since light is used to detected changes in the resonance frequencies, this measurement technique is known as Optically Detected Magnetic Resonance (ODMR) spectroscopy.

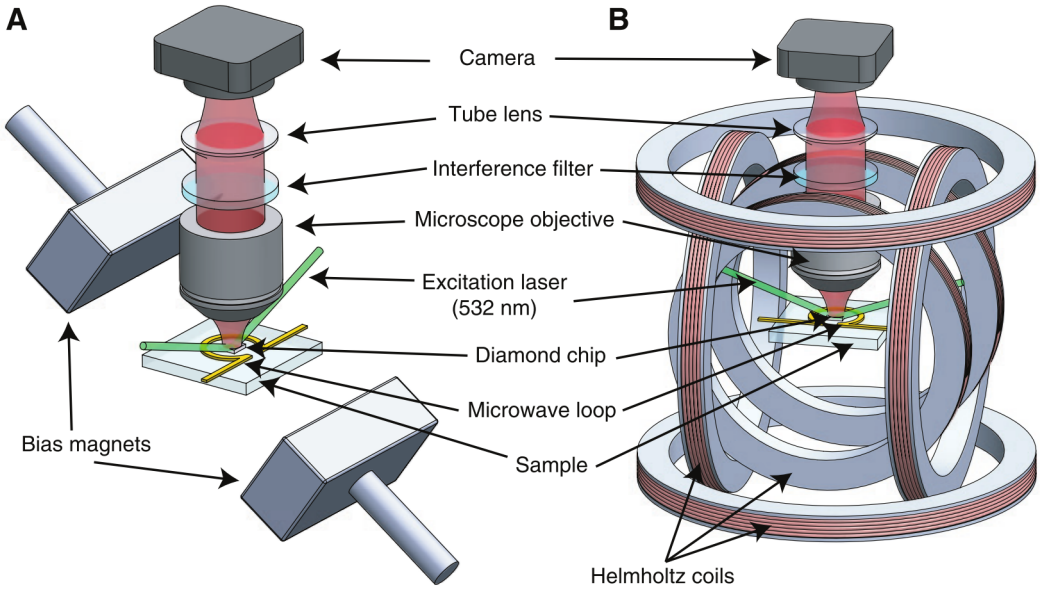

Figure 1.1: Schematics of two possible configurations of a Quantum Diamond Microscope. The different components work together to produce an image of the magnetic field of a sample that is held into place directly below the diamond crystal. Image taken from [**1**].

1.2 Optically Detected Magnetic Resonance Spectroscopy

Accurate measurement of the magnetic field of a sample relies on correct acquisition and interpretation of the information on its ODMR spectrum. Figure 1.2 shows an example ODMR spectrum that could be obtained from a QDM. The resonance dips present on the image correspond to features in the fine and hyperfine structure of the energy ground state of the NV center. In particular, the dips correspond to transitions of electrons in the ground state, going from the $m_s = 0$ level to the $m_s = \pm 1$ levels. Both of the $m_s = \pm 1$ feature three hyperfine energy levels.

When the frequency of the waves generated by the microwave loop matches the energy level difference between the ground state and one of these energy sublevels, electrons gain enough energy to transition to the upper energy level. The presence of electrons in the $m_s = \pm 1$ states reduces the amount of fluorescence detected by the QDM due to the properties of NV center (See section 2.1 for a more detailed description).

By comparing the ODMR spectrum obtained with and without a sample, it is possible to determine the magnetic field of the sample. Depending on the application, several protocols with different microwave and laser pulse sequences can be used. In this work,

we use the Continuous-Wave Optically Detected Magnetic Resonance (CW ODMR) protocol for magnetic field measurements.

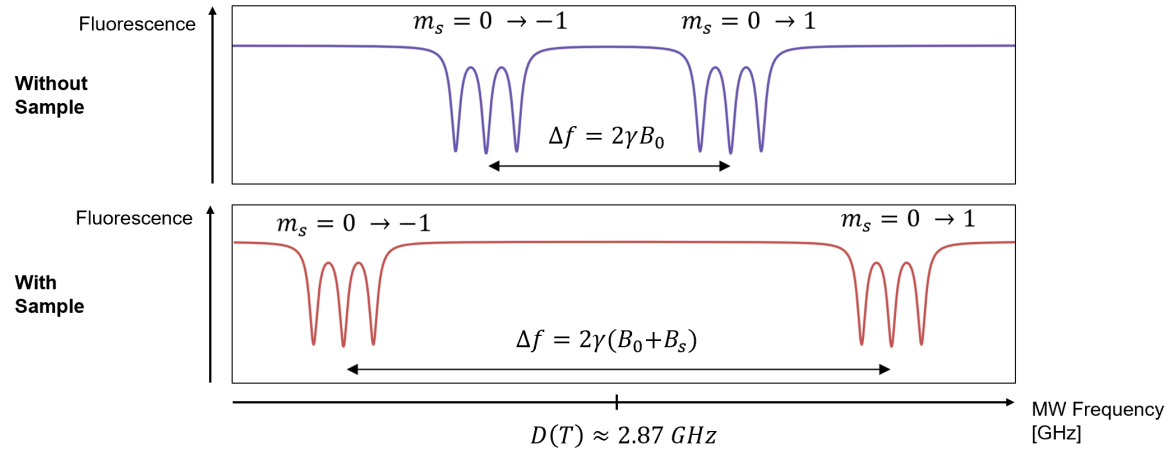

Figure 1.2: An example of an ODMR spectrum that can be obtained using a Quantum Diamond Microscope. The resonances are centered around the zero field splitting frequency $D(T) \approx 2.87$ GHz. The presences of a magnetic field causes a Zeeman shift, Δf, that is proportional to the magnetic field. $\Delta f = 2\gamma B_0$, where γ is the electron gyromagnetic ratio and B_0 is the magnetic field. When a sample with a magnetic field B_s is placed close to the NV diamond, the resonances are shifted. The magnetic field is determined in a very precise manner by measuring shifts in resonance frequencies.

1.3 Objectives

The goal of this project was to build, characterize, and use a QDM to measure magnetic fields. To determine the optimal experimental settings, we study the effects of the bias magnetic field, laser power, and microwave power on the ODMR spectrum. To characterize the QDM, we also study the background noise of our measurements as a function of measurement time. To demonstrate an application of the QDM, we measure the magnetic field of a solenoid. The objectives are described in more detail below.

The first objective was to study how different bias magnetic field directions produced by the Helmholtz coils affect the ODMR spectrum, and to choose the appropriate bias magnetic field for our QDM. To accomplish this objective, we need to first calculate the magnetic field produced by the Helmholtz coils and determine the current that needs to be applied to the coils to produce a desired bias magnetic field. Then, the ODMR spectrum can be measured at the various desired bias magnetic field orientations.

The second objective was to study the effects of laser power and microwave power on the ODMR spectrum and the magnetic field sensitivity of the QDM. To accomplish this objective, we need to develop a program to carry out the appropriate data analysis procedures.

The third objective was to measure the background noise of the QDM and monitor

how it improves with increased data collection time.

The fourth objective was to use the QDM to measure the magnetic field of a sample. As an example demonstration of the QDM, our goal was to measure the magnetic field of a solenoid actuator.

The rest of this report is organized as follows. Chapter 2 provides a description of NV centers, as well as of the physical principles underlying Optically Detected Magnetic Resonance Spectroscopy. Chapter 3 describes the components used to build the QDM with greater detail, the procedures used for data collection, and the data analysis. The results of the different measurements are shown and discussed in Chapter 4. The conclusions drawn from these results are listed in Chapter 5, along with suggestions for future research.

Chapter 2

NV Physics

2.1 Nitrogen-Vacancy Centers

Nitrogen-vacancy (NV) centers are defects in the crystalline structure of the diamond where a Nitrogen atom has taken the place of a carbon atom, and has caused a hole or vacancy on an adjacent location of the lattice. The vacancy is occupied by the free electrons on the lattice: NV centers with five electrons are neutral (NV^0), while those with six are negatively charged (NV^-). Most of the literature is focused on the negatively charged NV center in diamond [**2**].

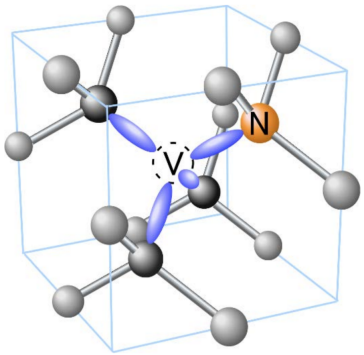

Figure 2.1: Nitrogen-Vacancy Center in a diamond crystal. The atoms neighboring the vacancy center are aligned in the corners of a regular tetrahedron centered in the lattice vacancy. Image taken from [**8**].

The Nitrogen-Vacancy center energy structure has four levels: The $^3A_2$ ground state, the ^3E excited state, and two intermediate transition states $^1A_1$ and ^1E, as shown in Fig.2.2. The ground and exited triplet states have a three-level fine structure for values of $m_s = 0$, $m_s = -1$ and $m_s = 1$. Each of these levels also has its own three-level hyperfine structure. These levels have a Zero Phonon Line (ZPL) of 637 nm. In contrast, the properties of the intermediate singlet states are less understood, although for the purposes of NV magnetometry it suffices to know that electron spin is not conserved during electron transitions through the singlet states.

The most important property of the NV center is in the nature of its photoluminescence. When illuminated with green light (532 nm wavelength), excited NV center

electrons with spin $m_s = 0$ emit red fluorescence when decaying back to the ground state, while NV center electrons with spin $m_s = \pm 1$ are more likely to follow an alternative nonradiative path via the intermediate energy levels. This non-radiative mechanism is known as an Intersystem Crossing (ISC)[**2**].

Since the amount of fluorescence emitted from the electron transitions depends on the number of electrons with a given spin, measuring changes in fluorescence from the NV centers in diamond effectively corresponds to measuring changes in the probability distribution of electron spin.

Electron spin transitions or "spin flips" can be induced on the electrons present on the NV center ground state by applying microwaves. Microwaves of frequencies around 2.87 GHz provide the right amount of energy to flip the spin of the electrons from the $m_s = 0$ state to the $m_s = \pm 1$ states. These electrons are then promoted to the $m_s = \pm 1$ levels of the excited state by the laser light, and become more likely to return to the ground state via the intermediate energy levels without emitting fluorescence. This idea underlies the optical detection principles of ODMR. It is possible to understand how microwaves can produce electron spin flip by studying the principles of Magnetic Resonance.

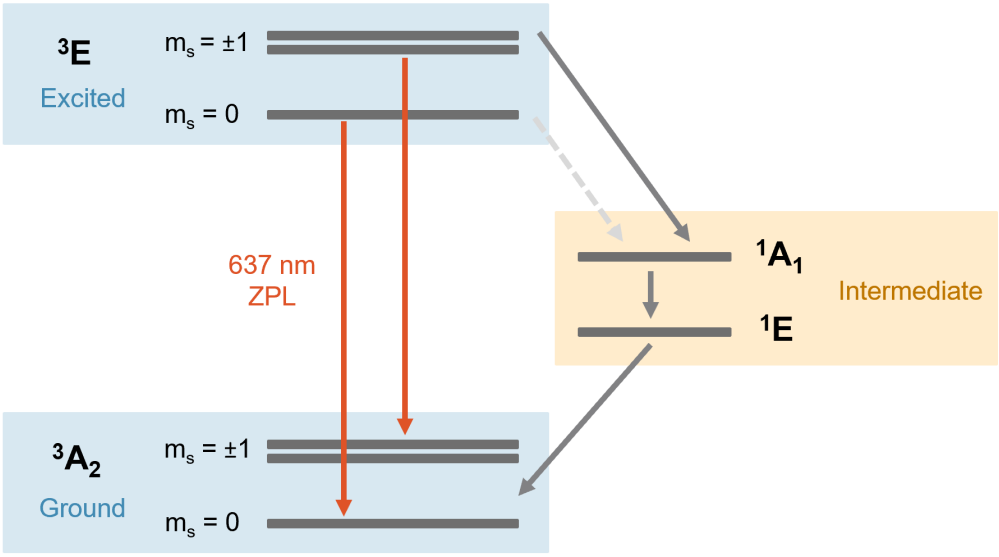

Figure 2.2: Energy Level Diagram for a NV Center. The arrows indicate the possible decay paths for electrons in the excited state. Electrons from the $m_s = \pm 1$ levels are much more likely to return to the ground state by going through the intermediate energy levels without emitting red fluorescence than electrons from the $m_s = 0$ levels.

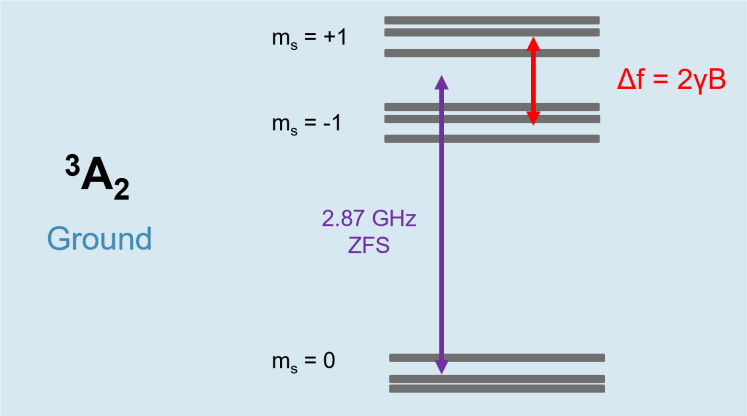

Figure 2.3: NV Ground State Hyperfine Structure. The average separation between the $m_s = 0$ and $m_s = \pm 1$ levels is represented by the Zero Field Splitting (ZFS) Frequency $D(T) \approx 2.87$ GHz. The spacing between the $m_s = \pm 1$ is levels is subject to the Zeeman Effect, and thus is dependent on the electron gyromagnetic ratio γ and the magnitude of the applied magnetic field B.

2.2 Magnetic Resonance

Magnetic resonance is a quantum phenomenon that arises in spin-1/2 particles that are under the influence of both a static and an oscillating magnetic field. Under such conditions, the particle experiences a great increase in the probability of spin flip when the frequency of the oscillating magnetic field approaches the Larmor Frequency, which is dependent on the magnitude of the static magnetic field.

When an electron, which is a spin-1/2 particle, is placed in a constant magnetic field $\boldsymbol{B_0}$, it experiences a torque that causes its spin vector to oscillate describing a circle in a plane normal to the direction of said magnetic field. This motion of the spin vector perpendicular to the applied magnetic field is known as Larmor precession. The Larmor Frequency ω_0 is proportional to the magnitude of the magnetic field and the electron's charge to mass ratio. In a QDM, the magnitude of the static magnetic field is mostly determined by the magnetic field generated by the Helmholtz coil array as well as the magnetic field of the sample that is being studied. The Larmor frequency is

$$\omega_0 = \frac{g_e e}{2m_e} B_0 = \frac{g_e \mu_B}{\hbar} B_0, \tag{2.1}$$

where $\hbar, g_e$ and μ_B are the reduced Planck constant, the electron g-factor, and the Bohr magneton, respectively. The addition of a secondary oscillatory field $\boldsymbol{B_1}$ in a direction perpendicular to the static magnetic field changes the physical description of the problem. In this case the values of the Larmor frequencies ω_0 and ω_1 are still relevant, but the direction of spin precession is mainly determined by the frequency of the oscillating magnetic field ω. In a QDM, this secondary magnetic field is provided by the microwave loop. As in the static case, the magnitude of he microwave magnetic field B_1 determines the value of Larmor frequency ω_1, while its oscillation frequency is ω.

In the context of NV magnetometry, the spin flip of interest is that of an electron going from the $m_s = 0$ sublevel to one of the $m_s = \pm 1$ levels of the energy ground state. This transition is directly correlated with the probability of an electron emitting fluorescence. The probability of this spin flip due to magnetic resonance is given by the Rabi formula [**3**, **9**].

$$P_{0\to\pm1} = \frac{\omega_1^2}{(\omega-\omega_0)^2+\omega_1^2}\sin^2\left(\frac{\sqrt{(\omega-\omega_0)^2+\omega_1^2}}{2}t\right) \tag{2.2}$$

When the frequency of the oscillating magnetic field approaches the Larmor frequency ω_0 the magnitude term in Equation 3 greatly increases, which gives rise to resonant behavior. ω_0 is therefore also known as the resonant frequency of the system. Since the QDM observes fluorescence coming from a large number of spin-flip transitions during a significant amount of time, the probability of transitions is expected to converge to $\langle P_{0\to\pm1}\rangle$.

$$\langle P_{0\to\pm1}\rangle = \frac{f_1^2}{(f-f_0)^2+f_1^2}, \tag{2.3}$$

where $\omega_n = 2\pi f_n$. The mathematical shape of this resonance curve is known as a Lorentzian. Since the electron energy levels of the NV have both fine and hyperfine structures, the probability of spin flip as a function of the microwave frequency will contain several Lorentzian line shapes added together, one for each of the hyperfine energy levels. Additionally, since the parameters f_0 and f_1 depend on the magnitude and direction of the static and oscillating magnetic fields, changes in these values will also change the probability of electron transitions at a particular microwave frequency. In particular, a Zeeman shift is expected to occur when a sample with a static magnetic field is placed near the diamond.

The QDM uses the principles of magnetic resonance in order to determine the magnitude of the magnetic field of a sample. When the sample is placed near the NV diamond, the change in the magnitude of the field produces a shift of the Larmor frequencies that is different from those obtained when there is no sample near the NV diamond. Since the Larmor frequencies are proportional to the magnitude of the applied magnetic field B, the magnetic field present on the NV diamond can be calculated by measuring the separation between the fine structure resonance peaks. The ODMR spectrum is usually obtained in the frequency range going from 2.80 to 2.94 GHz, which encompasses the range of all of the $m_s = 0$ to $m_s = \pm 1$ ground state transitions.

2.3 NV Center Hamiltonian

The relevant physics of NV centers can also be successfully described by considering the behavior of electrons on the ground state. Electrons on this state can occupy any of the three m_s sublevels. The energy of electrons on the NV center ground state, subject to a magnetic field $\boldsymbol{B}$ can be described by the Hamiltonian

$$
\begin{aligned}
H &= hD(T)S_z^2 - \boldsymbol{\mu} \cdot \boldsymbol{B} \\
&= hD(T)S_z^2 + g_e\mu_B(\boldsymbol{S} \cdot \boldsymbol{B}) \\
&= hD(T)S_z^2 + h\gamma(\boldsymbol{S} \cdot \boldsymbol{B})
\end{aligned}
\tag{2.4}
$$

,

where $D(T)$ is the Zero Field Splitting (ZFS) frequency, which depends on temperature, μ is the magnetic moment of the electron, $\boldsymbol{S} = (S_x, S_y, S_z)$ is a vector containing the spin-1 system dimensionless matrices, h is the Plank constant, and γ is the electron gyromagnetic ratio. This Hamiltonian formulation assumes the z-axis is pointing along the internuclear axis of the NV center [**6**].

It is also possible to formulate the Hamiltonian in a more compact form by introducing the Larmor Frequencies, which emphasize the role of angular momentum in the Hamiltonian. This particular form of the Hamiltonian is convenient for discussing spin precession and magnetic resonance.

$$
H = hD(T)S_z^2 + \hbar(\boldsymbol{\omega} \cdot \boldsymbol{S}) \tag{2.5}
$$

A complete Hamiltonian for an NV center involves several additional terms that account for the interactions between the Nitrogen nucleus and the electrons as well as internal electrical fields and crystal strain. In many practical cases the contributions of these terms are negligible and do not alter the principles of operation of the QDM, and therefore are not included here [**6**].

This Hamiltonian can be rewritten to match the form of the Hamiltonian of a spin-1/2 system in the cases where it is only of interest to analyze one of the possible electron transitions (i.e. $m_s = 0$ to $m_s = 1$) Substracting a term of $H/2$ from the Hamiltonian and focusing only on the $m_s = 0$ to $m_s = 1$ transition leaves us

$$
H = \frac{hD(T)}{2}\begin{pmatrix} 1 & 0 \\ 0 & -1 \end{pmatrix} + \frac{\hbar}{2}(\boldsymbol{\omega} \cdot \boldsymbol{S}) \tag{2.6}
$$

To illustrate how magnetic resonance gives rise to the features of the ODMR spectrum, we consider a simplified case of a sample with a static magnetic field $\boldsymbol{B_s} = B_s\hat{z}$ measured with a QDM with a bias magnetic field $\boldsymbol{B_0} = B_0\hat{z}$ (generated by the Helmhholtz Coils). In order to induce spin flips, microwaves represented by an oscillating magnetic field $\boldsymbol{B_1} = B_1 cos(\omega t)\hat{x} + B_1 sin(\omega t)\hat{y}$ are introduced. Under these circumstances the Hamiltonian becomes [**3**].

$$
\begin{aligned}
H &= \frac{\hbar}{2}\begin{pmatrix} 2\pi D(T) + \omega_0 & \omega_1 e^{-i\omega t} \\ \omega_1 e^{i\omega t} & -2\pi D(T) - \omega_0 \end{pmatrix} \\
&= \frac{\hbar}{2}\begin{pmatrix} \omega_0' & \omega_1 e^{-i\omega t} \\ \omega_1 e^{i\omega t} & -\omega_0', \end{pmatrix}
\end{aligned}
\tag{2.7}
$$

where the Larmor Frequencies $\omega_n = g_e\mu_B B_n/\hbar$ and the shifted frequency $\omega_0' = 2\pi D(T) + \omega_0$ have been introduced. This is the simplest Hamiltonian that can be used

to describe the QDM operation using the principles of the magnetic resonance. It leads to the spin flip probability equation (Eq. 2.3).

$$\langle P_{0\to\pm1}\rangle = \frac{f_1^2}{(f-f_0')^2+f_1^2}, \tag{2.8}$$

where the resonance frequency is

$$\begin{aligned} f_0' &= D(T) + \frac{g_e\mu_B}{h}B_z \\ &= D(T) + \gamma B_z \end{aligned} \tag{2.9}$$

Since $B_z = B_0 + B_s$ the magnetic field of the sample of interest can then be calculated by measuring the difference in the the value of f_0' obtained with and without the sample, as it was shown on Figure 1.2.

The derivation shown here is applicable for the $m_s = 0 \to m_s = 1$ transition. However, due to symmetry of the Hamiltonian the same frequency shift holds for the $m_s = -1$ transition. Therefore, the difference between the two frequency peaks when there is a magnetic field applied in the $\hat{z}$ direction is

$$\Delta f = 2\gamma B_z = B_z \cdot 5.60 \text{ MHz/G} \tag{2.10}$$

The analysis of the ODMR spectrum to determine resonance frequencies can then be carried out by curve-fitting the data of each of the hyperfine resonances to the equation.

$$y_{hf}(f) = 1 - C_{hf} \cdot \frac{f_1^2}{(f-f_0')^2+f_1^2} \tag{2.11}$$

where the hyperfine structure contrast C_{hf} value is a parameter that can be adjusted during the fitting process, and represents the maximum drop in fluorescence, which is achieved at the resonant frequency.

This exercise on magnetic resonance allows us to make several predictions about the behavior of the ODMR spectrum:

1. Power Broadening: An increase in the magnitude of the microwave power will generate an increase of the magnitude of the magnetic field B_1 and as well as of its respective Larmor frequency, which will in turn cause the resonance peak to spread out to encompass a greater range of frequencies.

$$f_1 \propto \sqrt{P_{MW}} \tag{2.12}$$

2. Resonance Peak Amplification: Increased laser power is expected to produce more electron energy transitions, and thus increase the amplitude of the resonance peaks, but without producing significant power broadening (within the power limits of our experiment).

$$C_{hf} \propto P_{Laser} \tag{2.13}$$

3. ODMR Center Frequency Shift: Increased laser power will also produce a proportional increase in the temperature of the diamond. Thus, due to the temperature dependence the Zero Field Splitting Frequency, higher laser power will result in a lower Zero Field Splitting. This is described by the equation below (T is temperature in Kelvin) [**6**].

$$D(T) = 2.87 \text{ GHz} - \Delta T \cdot 74.2 \text{ kHz/K} \tag{2.14}$$

We observe these behaviors in our experiments described in Chapter 4.

Chapter 3

QDM Experiment Set-up and Operation

3.1 QDM Experiment Components

In this chapter, we describe the relevant information about the hardware components used in the QDM we constructed, the measurement procedure, and the data analysis procedure. First, the key components of the QDM mentioned in Ch.1 are describe here in more detail. For reference, a diagram of the main components of the QDM is shown in Figure 3.1. The key components are seen on the right of the diagram. These are the laser, Helmholtz coils, microwave loop, and camera. The NV diamond, not shown in the Fig. 3.1, is also a crucial component. The NV centers in the diamond are the quantum sensors. The laser is used to excite the NV centers. The camera is used to collect the red fluorescence emitted by the NV centers. The microwave loop is used to control the spin states of the NV centers. The Helmholtz coils are used to produce a bias magnetic field at the NV centers. These specific components of the QDM we build are described in more detail in the subsections below.

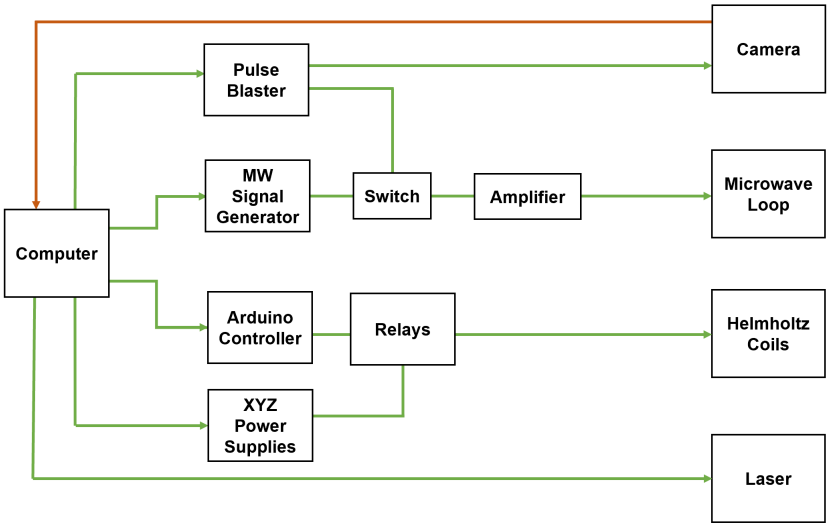

Figure 3.1: Diagram showing the connections between the different subsystems of the QDM.

3.1.1 NV Diamond

A 4 by 4 by 1 mm rectangular diamond with approximately a 1.5 micron layer of NV centers was used in order to carry all of the measurements in this report. The diamond lattice contains an ensemble of Nitrogen-vacancy centers oriented in four separate directions. Due to the geometry of the diamond lattice, the location of a Nitrogen atom in an NV center can only be along one of four possible directions with respect to the vacancy center. These directions are referred to as the diamond NV axes. They are shown in Fig. 3.2.

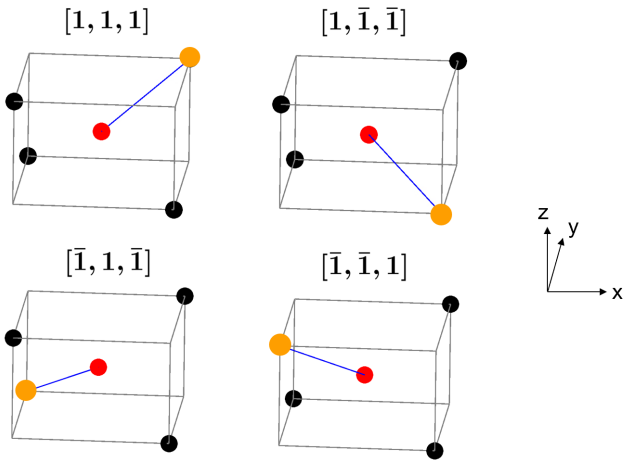

Figure 3.2: Diamond NV Axes. The red dot represents the vacant spot located within the center of a cell of the diamond crystal lattice. Carbon and Nitrogen atoms are represented by black and orange dots, respectively.

3.1.2 Laser

Green laser light (532 nm wavelength) provided the necessary energy to excite the NV centers. A Sprout-H Series laser from Lighthouse Photonics was used in our QDM. The laser was directed with mirrors through a half waveplate, that was used to control the laser polarization, and a lens, that was used to change the size of the beam, before hitting the NV diamond. An image of the NV diamond illuminated by the laser is shown in Fig. 3.3.

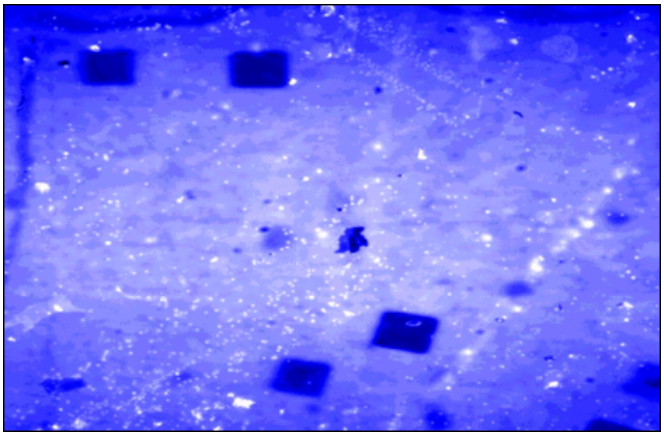

Figure 3.3: Image of the central region of the NV diamond taken by the QDM camera, illuminated by the laser light.

3.1.3 Camera and Imaging Optics

A 4x magnification microscope objective and 100 mm focal length tube lens are used to image the fluorescence from the NV centers onto a Basler acA-1920-155μm camera. An optical filter that only transmit wavelength above 650 nm is placed before the camera to prevent green laser light from hitting the camera sensor. The camera has 1920 by 1200 pixels. For each experimental trial the range of view of the camera was adjusted in order to collect fluorescence coming from the region directly illuminated by the laser in the center of the NV diamond, as shown in Fig. 3.3. The exposure time also needs to be adjusted for different laser powers to prevent the camera from being light saturated. Typical values for the exposure time for different laser powers are shown in Fig. 3.1.

Laser Power [W]	0.5	1.0	1.5	2.0	2.5	3.0
Exposure Time [ms]	350	150	100	80	60	45

Table 3.1: Camera exposure time used for different laser powers.

3.1.4 Microwave Field

A thin U-shaped Copper wire was placed close to the diamond surface to serve as the microwave source in charge of delivering microwaves to the NV centers. Microwave frequencies ranging from 2.80 to 2.94 GHz were generated with a the frequency signal generator and sent to the microwave loop. The microwave power was also be controlled, ranging from -25 to 5 dBm.

3.1.5 Bias Magnetic Field

Three axis Helmholtz coils are used to produce a bias magnetic field at the NV diamond. The magnitude and direction of the bias magnetic field affects the values of the resonant frequencies in the ODMR spectrum, and therefore plays a major role in the features of ODMR spectrum. This field can be adjusted by controlling the amount of current that flows through each of the Helmholtz Coils. The direction of the bias

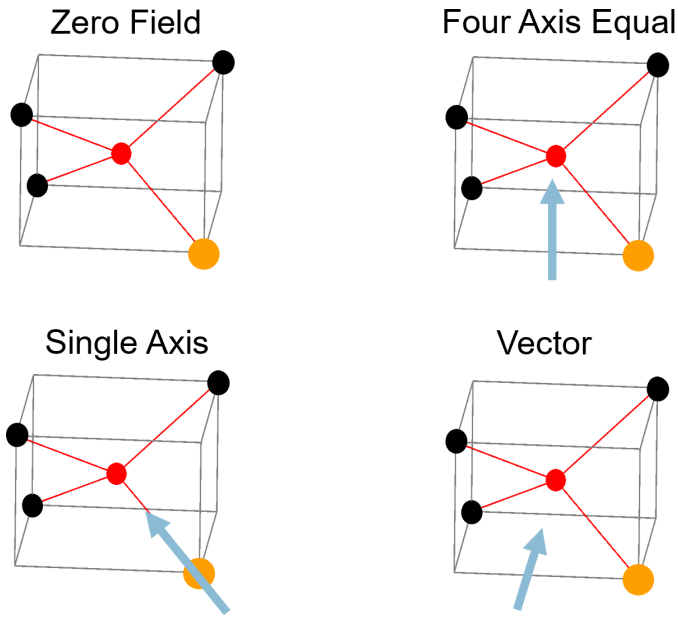

Figure 3.4: Possible bias magnetic field configurations with respect to the internal structure of the NV Center. The red dot represents the vacant spot located within the center of a cell of the diamond crystal lattice. Carbon and Nitrogen atoms are represented by black and orange dots, respectively. The blue arrow indicates the direction of the bias magnetic field on each configuration.

magnetic relative to the orientation of the diamond lattice alters the ODMR spectrum because it may cause degeneracy of the energy levels. The different bias magnetic field configurations relative to diamond NV axes are classified into four groups. These are Zero Field, Single Axis, Four Axis equal, and Vector Field configurations. They are shown in Fig. 3.4 and described below.

For the Zero Field configuration, there is no magnetic field at the NV diamond.

The Four axis equal direction or NV internuclear axis direction is the one in which the bias field projection into each of the four NV axes is the same. Due to the cubical structure of the diamond lattice, this configuration can be obtained using six different bias field alignments.

Measurements along the single axis direction are obtained by aligning the bias magnetic field along one of the NV center axes. Since there are only four NV axes, it is possible to make this kind of measurement using eight different magnetic bias magnetic field configurations. This causes the energy levels for NV centers oriented along the other three axes to be degenerate. A single axis measurement yields an ODMR Spectrum with four fine structure resonance peaks. This particular configuration is of interest because the Zeeman Shift of the outer two resonances obtained in with a bias magnetic field in this configuration is proportional to the magnetic field component along that NV axis. As such, it is the most common configuration used for measuring magnetic fields of a sample of interest.

A measurement that is carried out with a bias magnetic field direction different from the zero field, four axis, or single axis configurations will result in non-degenerate energy levels for NV centers along each of the four possible NV axis directions. This is known as a vector bias magnetic field configuration because it can allow us to measure all three components of the magnetic field of a sample at the same time. However, this configuration has some limitation due a more complex ODMR spectrum where it may not always be clear which resonance correspond to NV center along each of the orientations.

The magnetic field generated at the center of the Helmholtz Coil set up can be calculated with using the Biot-Savart Law. A standard textbook calculation yields an expression for the magnetic field B at a point located a distance z away from the center of n closely winded loops of current of radius R [**4**].

$$B = n\frac{\mu_0 I}{2}\frac{R^2}{(R^2+z^2)^{3/2}} \tag{3.1}$$

where I is the current on the loop of wire and μ_0 is the permeability of vacuum. This equation can be used to calculate the contributions from each of the Helmholtz coil loops, which can the be added together to obtain the resulting magnetic field. The effect of the Earth's magnetic field is not negligible, and thus its magnitude and direction need to be known in order to properly calculate the amount of current that must go through each of the Helmholtz coil loops. Using information provided by the National Oceanic and Atmospheric Administration (NOAA) the magnetic field of the Earth was determined to be of a strength of 51.7 μT, with a predominant downward component. Accurately determining the direction of total magnetic field at the center of the QDM with respect to the direction of the NV axes inside the diamond crystal is essential in order to ensure that the Zeeman Shift of the resonant frequencies is directly proportional to the magnetic field of the sample placed near the diamond.

The current values used to generate the magnetic field of the Helmholtz coils were calculated using a MATLAB program that used the Biot-Savart Law and the components of Earth's magnetic field at the lab location to determine the orientation of the different NV axes on the diamond crystal.

Helmholtz Coil Current [mA]	Zero Field	Single Axis	Vector	Four Axis Equal
x	-36.2	-40.0	350.3	-36.2
y	-15.0	-2280	-1336.9	-15.0
z	89.4	-1310	2343.3	2343.3

Table 3.2: Helmholtz Coil current values used to obtain different bias magnetic field configurations.

Magnetic Field Values [μT]	Zero Field	Single Axis	Vector	Four Axis Equal
x	0	-1.9	200	0
y	0	-1199.4	-700	0
z	0	-745.0	1200	1200
Magnitude	0	1411.9	1403.6	1200

Table 3.3: Generated Bias Magnetic Field values.

3.2 Measurement Procedure

In order to conduct a measurement, the sample of interest is placed near the NV diamond. The laser is directed to illuminate the NV diamond, which is at the center of the Helmholtz Coil array. The laser provides the energy necessary to make the electrons in the NV diamond move to an excited energy level, while the camera collects the fluorescent light coming from the decay of the electrons back to the ground state. The Helmholtz coils and microwave loop are used to generate the appropriate conditions for magnetic resonance in the NV centers.

Before conducting a measurement, the NV diamond must be properly aligned below the microscope objective. This is done with the aid of a "Camera Viewer" program on the QDM computer that displays the image recorded by the camera on real time. The program allows the user to observe the NV diamond surface and select a region in which to conduct the measurements. For best results, measurement must be made on a region evenly illuminated by the laser light and free from defects. The Camera Viewer also allows the user to adjust the camera exposure time, which determines the amount of light that enters the camera per measurement frame. For a proper measurement to be made, the camera should not be saturated.

Once the optical parameters have been adjusted, the necessary bias magnetic field must be generated. This is done by another Labview program that controls the currents sent from the power supplies to each of the x,y, and z Helmholtz Coils. The current values needed in order to generate the desired bias magnetic field are discussed in section 3.1.5. For most measurements, we use the single axis bias magnetic field configuration.

The experiment data collection is handled by a Labview QDM data collection program, which was created specifically for collecting ODMR data. The microwave power and frequency range are inserted as inputs. The desired optical parameter values are also inserted, including coordinates for indicating the diamond region to be analyzed. The program also allows the user to select different data collection parameters, such as the number of microwave frequencies and the amount of data to collect, and to supervise the experiment in real time.

Data collection by the QDM program works by recording the amount of fluorescence collected by the camera at each individual pixel. During a measurement, fluorescence is collected at a finite number of different microwave frequency values, which are selected to be in the range where the resonance peaks of interest are located. Alternating measurements are taken with microwaves turned on at the desired frequency and then off as a

reference so that the fluorescence can be normalized. Several iterations of these frequency sweeps are carried out and averaged in order to accurately construct the shape of the ODMR spectrum of each pixel in the frequency range of interest. This information is then stored into a large three-dimensional MATLAB array, which can then be loaded by a MATLAB program to study the fluorescence of different pixels at different microwave frequencies.

To ensure that the hyperfine peaks on the ODMR spectrum could be clearly resolved, data points were collected near the resonance peaks of interest with a maximum separation between neighboring microwave frequencies of 360 kHz. The number of frequency sweeps collected and averaged was chosen such that the data could be analyzed with the necessary precision and accuracy. The effect of measurement time or number of sweeps on the measurement noise is discussed in Section 3.3.1 and Section 4.3.

In addition to collecting individual pixel data, the QDM Labview program also displays a plot of the "Global ODMR" spectrum, as shown in Fig. 3.4, which is obtained by doing a cumulative average of the individual pixels' fluorescence values, through different iterations. This plot was used to initially set-up the desired experimental parameters and then used to monitor data collection in real time.

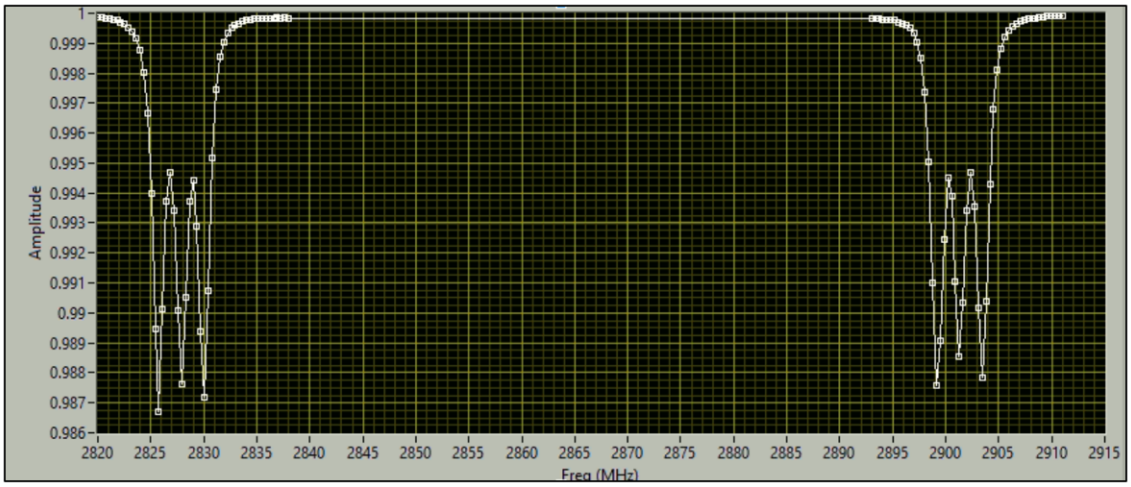

Figure 3.5: Image of the global ODMR spectrum collected by Labview program. Data points are collected near the resonance peaks of interest.

3.3 Data Analysis

The Graphics Processing Unit of the QDM computer is used for fitting the ODMR data in MATLAB. The sum of three Lorentzian functions is used to fit each resonance to take into account the hyperfine structure observed in the ODMR spectrum. From the discussion in Chapter 2, we showed that a single resonance can be described by a Lorentzian in Eq. 2.11. Since the hyperfine resonances are located very close together, it is necessary to define the fitting function, $y_f(f)$, that is constructed by adding three hyperfine Lorentzians.

$$y_f(f) = 1 - \sum_{i=1}^{3} C_{hf}^{(i)} \frac{{f_1^{(i)}}^2}{\left(f - {f_0^{(i)}}'\right)^2 + {f_1^{(i)}}^2} \tag{3.2}$$

where $C_{hf}^{(i)}$ is the contrast, $f_1^{(i)}$ is the linewidth, and $f_0^{(i)}$ is the resonance frequency. The indices are used to denote the differences in the center frequency, width and contrast of the individual Lorentzians corresponding to the hyperfine structure. An example of the fit function showing the three Lorentzians separately is in Fig. 3.6.

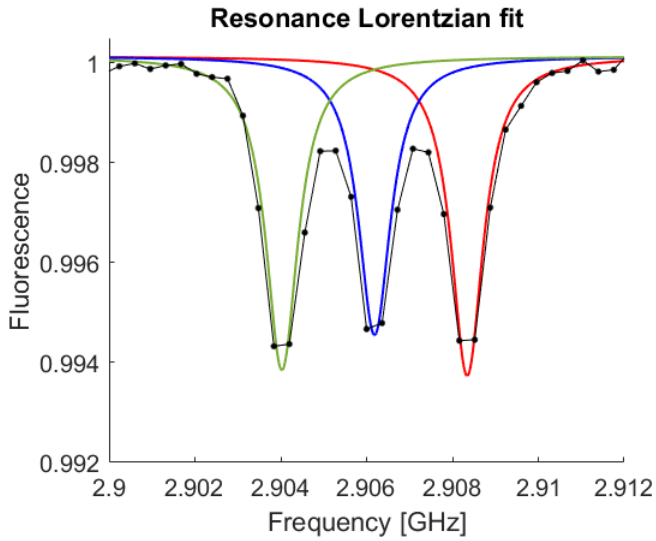

Figure 3.6: Sample ODMR Data Analysis in MATLAB. Measured data points are shown in black. The green, blue, and red lines are the three Lorentzians fit to each hyperfine feature in the data. The full resonance is fit by the sum of the three Lorentzians shown.

The resulting parameter values obtained by the fitting function for $C_{hf}^{(i)}$, $f_1^{(i)}$, ${f_0^{(i)}}'$ can then be used to accurately calculate the separation between two fine structure resonances Δf and obtain the magnitude of the applied magnetic B field using the equation.

$$\Delta f = 2\gamma B \tag{3.3}$$

Since the computer collects ODMR information from each pixel, the magnetic field magnitude value obtained from Eq. 3.3 can be used along with the pixel's coordinates in order to observe changes in magnitude of the field across the field of view captured by the camera. This allows us to observe changes in the spatial distribution of the magnetic field of the sample being measured.

The fitting parameters of each resonance can also be saved by the computer and be used later to conduct other types of additional analysis, as was done to process the data from the measurements described in Chapter 4. In some of the measurements, the fitting parameters values of the Global ODMR spectrum for each measurement were saved in individual MATLAB files which could then be used in order to produce an averaged image that showed how the fitting parameters changed as a function of microwave power and laser power.

3.4 Magnetic Field Sensitivity

In order calculate the minimum magnetic field variation that can be observed with a QDM, the sensitivity parameter is often used. A lower value for sensitivity means that a smaller magnetic field can be detected. For a QDM operating using a continuous wave protocol (CW-ODMR) the volume-normalized sensitivity (with units of $T\mu m^{3/2}Hz^{-1/2}$)is given by

$$\eta_{cw} = \frac{4}{3\sqrt{3}} \frac{h}{g_e \mu_B} \frac{\Delta\nu}{C_f\sqrt{R}}, \tag{3.4}$$

where $\Delta\nu$ and C_f are the linewidth and contrast of the resonance peak, respectively (as shown in Fig. 3.6), and R is the photon detection rate from a cubic micrometer of NV centers.

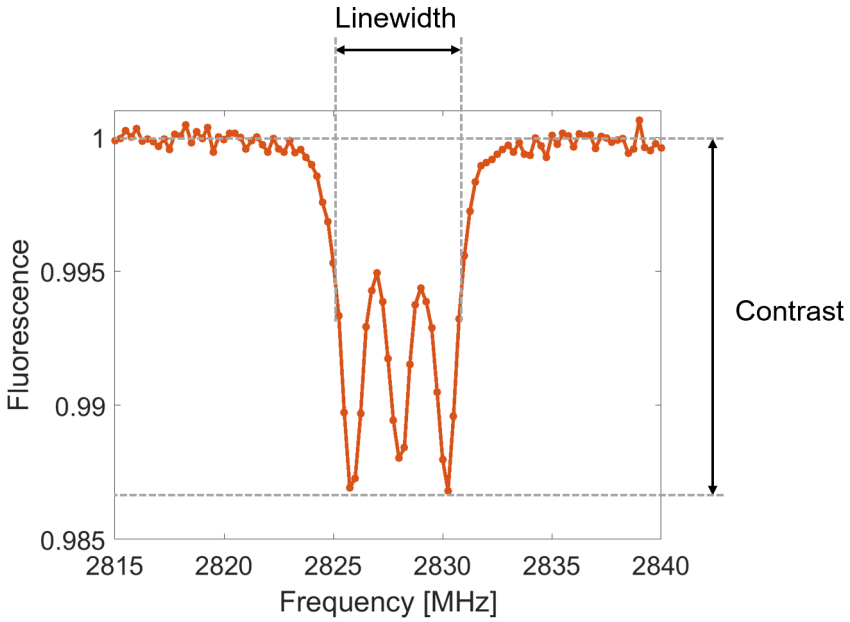

Figure 3.7: Contrast C_f and Linewidth $\Delta\nu$ of a fine structure resonance.

The values of linewidth and contrast can be calculated from the fit parameters describe in Eq.3.3 by the following equations.

$$C_f = \frac{1}{3}(C_{hf}^{(1)} + C_{hf}^{(2)} + C_{hf}^{(3)}) \tag{3.5}$$

$$\Delta\nu = f_1^{(1)} + f_1^{(2)} + f_1^{(3)} \tag{3.6}$$

Because the value of R is complicated to determine experimentally, an alternative figure of merit is defined, where the camera exposure time t_{Exp} is used instead. It is assumed that $t_{Exp} \propto 1/R$. This is done by first introducing the quantity η_{FOM}

$$\eta_{FOM} = \frac{\Delta\nu\sqrt{t_{Exp}}}{C_f} \tag{3.7}$$

Using this metric, lower sensitivity values correspond to higher magnetic field resolution. In order to help identify the optimal sensitivity value, the values obtained using the expression 3.7 were adjusted and normalized in order to produce a sensitivity figure of merit η^*_{FOM}, where the maximum value of 1 corresponds to the best sensitivity value.

$$\eta^*_{FOM} = \frac{\max(\eta_{FOM})}{\eta_{FOM}} \tag{3.8}$$

Chapter 4

Experiment Results

Three different experiments were conducted in order to fulfill the research objectives of characterization of the Continuous-Wave ODMR spectrum and the QDM. These were designed to study the effect of the 1) bias magnetic field, 2) microwave power and laser power in the ODMR spectrum, as well as 3) the background noise of the QDM. The QDM was then tested in a real-life application, measuring the magnetic field of a solenoid actuator.

The nominal experimental settings were a single axis magnetic field configuration, 2.5 W of laser power, and -10 dBm of microwave power. Some of the setting were varied for experiments that were intended to test either different bias field configurations or the effects of laser power and microwave power. For the bias magnetic field measurements, the Global ODMR spectra obtained were plotted and compared with previous experimental results [**1**]. In the remaining experiments the value of the magnetic field acting on the diamond was calculated by the MATLAB program and data analysis procedure described in Chapter 3.

4.1 Bias Magnetic Field Measurements

The first objective of this investigation was to observe the effect different bias magnetic field configurations had on the ODMR spectrum. The first step towards achieving this goal was the creation of a MATLAB program for calculating the currents necessary to obtain the different desired bias magnetic field configurations, which was mentioned in Section 3.1.5. Having developed the program, different images of the ODMR spectrum using the calculated current values in Table 3.2 were collected. The ODMR spectrum data for the four different bias magnetic field configurations are shown on Figure 4.1.

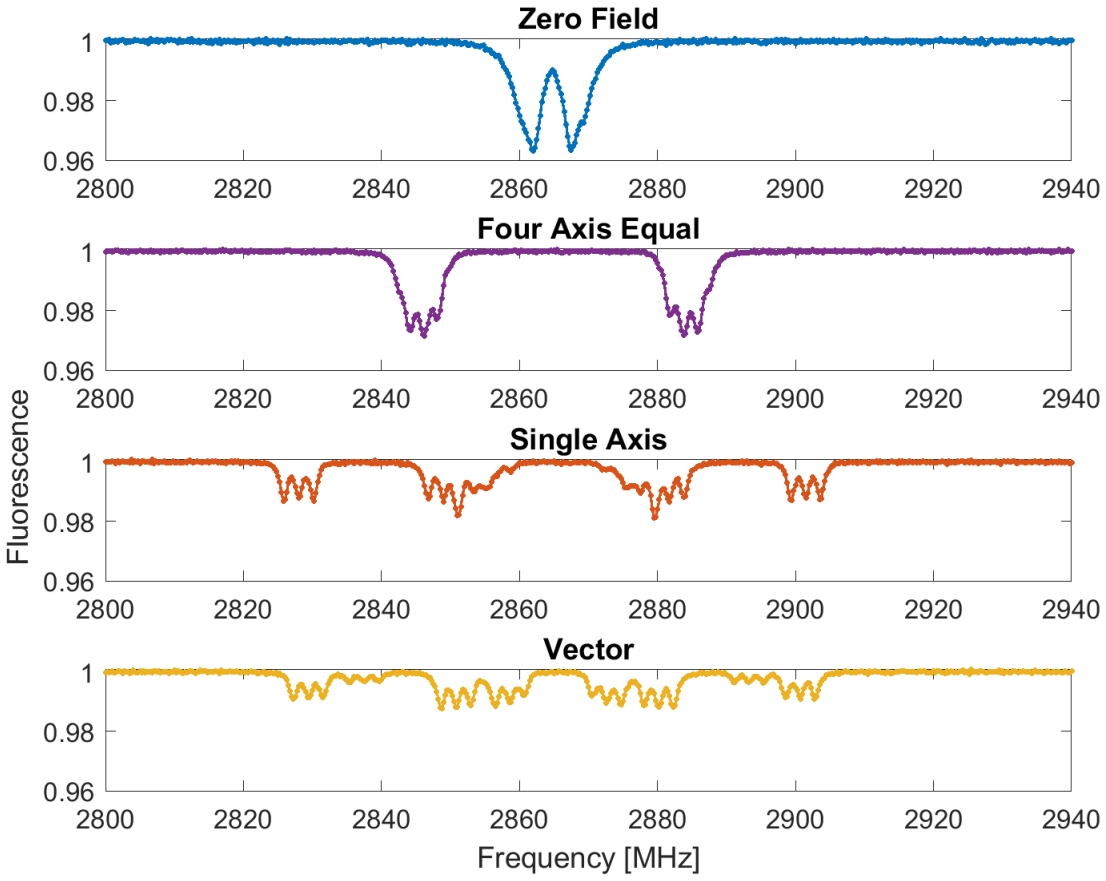

Figure 4.1: ODMR Spectrum measurements along different Bias Magnetic Field configurations.

The resulting ODMR spectra for the different magnetic field measurements were observed to be consistent with results from previous experiments [**1**] and consistent with our understanding of the NV physics. In the absence of an external magnetic field Zeeman splitting does not occur, and thus the $m_s = \pm 1$ resonances were seen to overlap very closely at 2.87 GHz, with a difference of about 5 MHz difference between their peaks. The introduction of a magnetic field pointing in the internuclear axis direction (also known as the Four-axis equal direction) gives rise to a separation of $m_s = \pm 1$ resonances, and also gives rise to some hyperfine structure details. A magnetic field pointing along the direction of one of the four diagonals of the cubical crystal lattice yields a single axis ODMR spectrum. This change in the direction of the magnetic field breaks down the degeneracy of the resonances seen on the Four-axis equal measurement. In this case, the outer two resonance peaks correspond only to the NV centers oriented along the bias magnetic field direction. The two inner resonance peaks are the degenerate resonances of NV centers with the other three orientations. Magnetic field measurements of a sample of interest are usually carried out in this single axis configuration. The shift in the outer two resonance peaks is used to calculate the magnetic field of the sample, while the two inner ones are discarded, as they correspond to other degenerate energy levels. Directing the bias magnetic field vector along any other direction yields a vector ODMR spectrum, which was observed to show eight fine structure resonance peaks.

4.2 Microwave and Laser Power Measurements

A study of the effect different microwave power and laser power on the shape of the resonances of the ODMR Spectrum was carried out. This was done by conducting a large number of measurements at different microwave and laser power values, which where then processed with the aid of several MATLAB programs that were designed for this purpose. The programs developed were used, among other things, to fit the raw global ODMR spectrum data points to a fitting function $yf(f)$ in order to be able to quantify the ODMR spectrum changes.

Measurements were made in the range of -25 to 5 dBm of microwave power and 0.5 to 3.0 W of laser power. Among the parameters studied were the contrast and the linewidth, as well as the sensitivity figure of merit η^*_{fom}, which were discussed in Section 3.4.

The behavior of the contrast and linewidth as a function of laser power and microwave power shown in the data in Fig.4.2 was consistent with the predictions made in Chapter 2. As a general trend, larger linewidth values were obtained at higher microwave power as a result of power broadening. This effect is most noticeable at the low laser power values. Contrast amplification was also observed at greater laser power values in

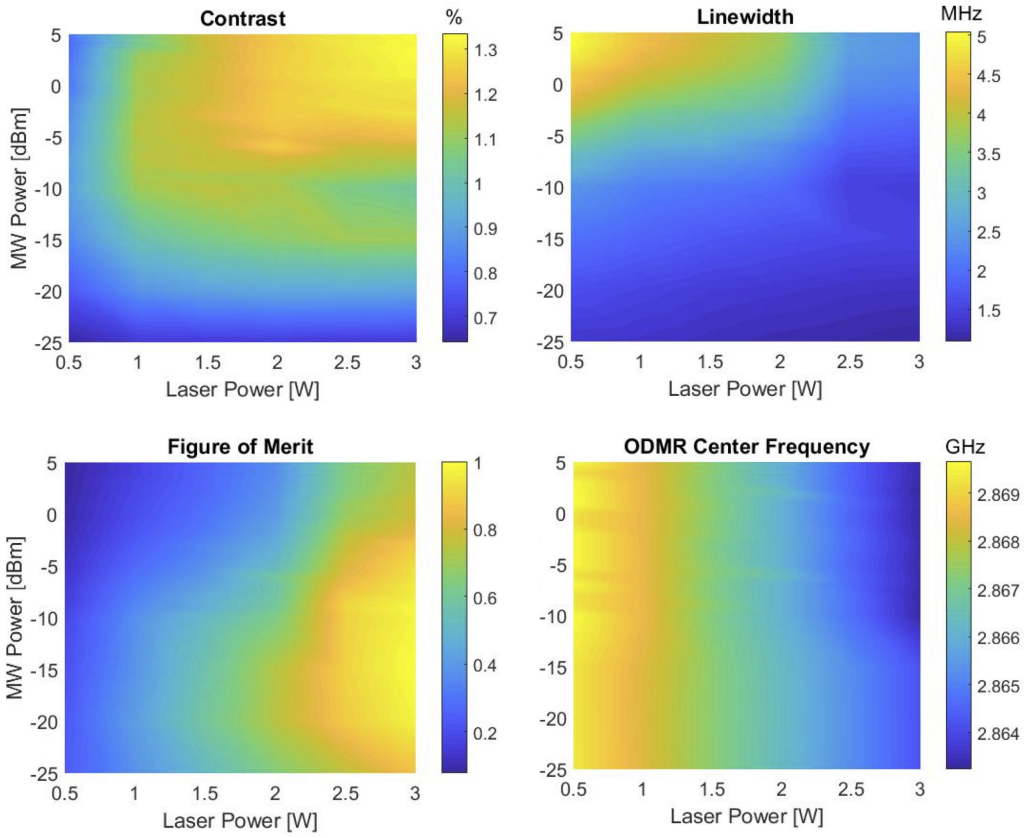

Figure 4.2: Analyzed data of the ODMR Spectrum Contrast, Linewidth, Sensitivity Figure of Merit, and Center Frequency Shift due to laser heating.

the microwave power range going from -15 to 5 dBm.

From the analyzed data shown in Fig. 4.2, we observe that the best magnetic field sensitivity was obtained around -15 dBm of microwave power and 3 W of laser power. Future experiments can be conducted with even higher laser power to test if the sensitivity would continue to improve for laser power above 3W.

The final observation was that the center frequency of the ODMR spectrum was shifted due to the heat generated by the laser light on the NV diamond. This particular effect does not alter the magnitude of the Zeeman shift between neighboring resonances, but does shift them by the same amount on the same direction. This center frequency resonance shift is accounted for by the temperature dependent term $D(T)$ in the Hamiltonian described in Chapter 2. This frequency shift was observed to be present across all microwave power values as the laser was the dominate source of heating in the experiments.

A more rigorous measurement of the effect of microwave and laser power on the ODMR spectrum requires considering several different factors, including transmission line effects on the MW loop circuit, the geometry of the microwave loop and its proximity to the diamond, as well as the laser polarization and incidence angle [**5**]. Moreover, the data collected for the sensitivity figure of merit suggests the possibility that greater resolution can be obtained by conducting measurements with higher laser power values.

4.3 Noise Measurements

The third objective of this investigation was to observe the effect data collection time on the background noise. Measurements of the ODMR spectrum without any samples present were made during periods lasting one, four, and eight hours in order to estimate the amount of error in magnetic field measurements due to the background. The measurements were taken at values of 2.5 W and -10 dBm of laser and microwave power, respectively.

The magnitude of the background noise was determined by calculating the standard deviation of the measured magnetic field of a 135 by 95 area of camera pixels. Figure 4.3

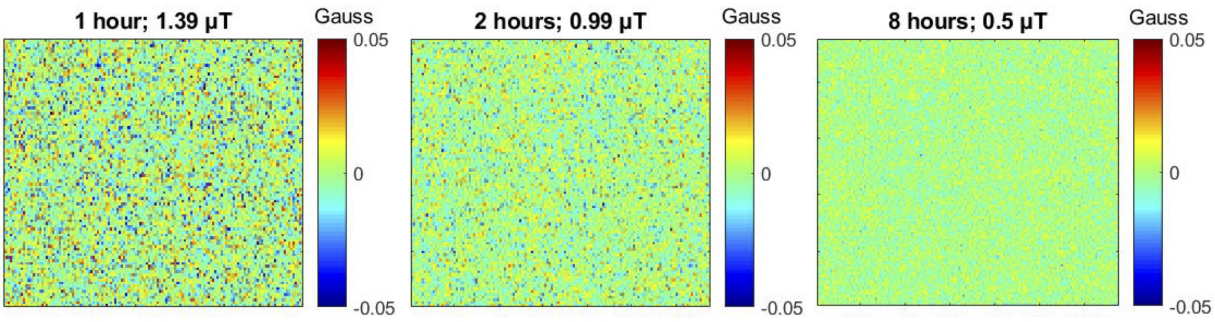

Figure 4.3: Background Noise measurement results after 1, 2 and 8 hours.

shows images of the magnetic field over the chosen field of view for different data collection times. As expected, the measurement results indicated that data collection during long periods of time helped to significantly reduce the amplitude of the background noise. The noise was reduced below $1\mu T$ after two hours of measurement, and to $0.5\mu T$ after 8 hours. This information, combined with the results of the sensitivity measurement are important for determining the experimental error bars in a magnetic field measurement.

4.4 Solenoid Measurements

The final component of this investigation was to test the QDM by imaging the magnetic field of a sample, which was a solenoid actuator. The actuator, STA Pull DC Tubular Solenoid Model 51, was provided by a Thomas Lipkin, who was interested in using the solenoid to control the movement of a prosthetic tongue (as part of another MQP at WPI).

The solenoid was placed vertically at a distance of approximately 11mm below from the diamond sample. Measurements were taken for about 20 minutes at values of 2.5 W and -10 dBm of laser and microwave power, respectively, and with the solenoid turned on and off. The magnetic field measurements of the on and off states as well as the their difference are shown in Fig. 4.4. A background gradient due to inhomogeneous laser illumination, microwaves, and bias field across a several millimeter field of view can also be seen the data in Fig. 4.4. Importantly, the data show that the QDM was able to detect a difference in the magnetic field between the solenoid on and off states. The measured result for the solenoid is a magnetic field of 0.75 ± 0.08 Gauss or $75 \pm 8\ \mu T$ along the NV axis at a distance of about 11 mm with a current of 90 mA through the solenoid.

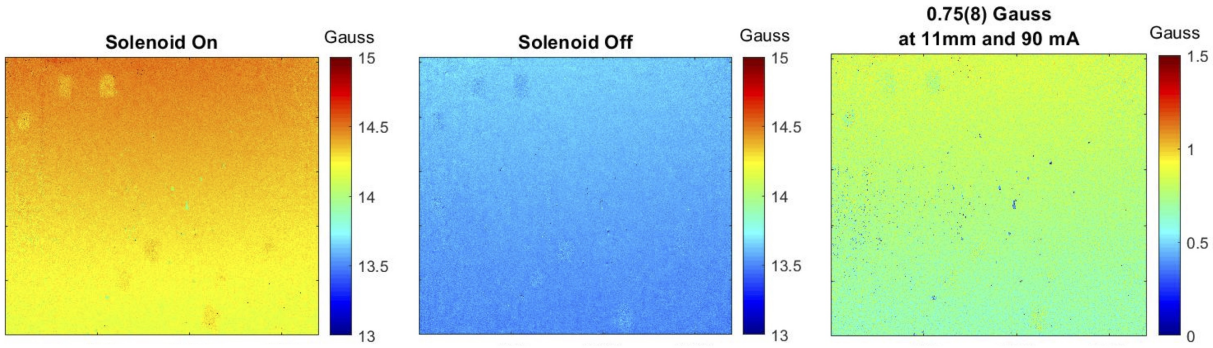

Figure 4.4: Results of the solenoid magnetic field measurement. The solenoid was placed 11mm away from the diamond. A difference of about 0.75(8) Gauss was detected between the two measurements when a current of 90 mA was used.

Chapter 5

Conclusions and Future Work

In this work, a QDM was successfully constructed and characterized. Changes in the shape of the ODMR spectrum shape were measured as a function of the bias magnetic field as well as the microwave and laser power. The changes observed in each of the different configurations were observed to be consistent with the predictions made based on the principles of magnetic resonance. A sensitivity figure of merit was defined and optimal experimental setting for laser power and microwave power of -15dBm and at least 3W, respectively, were recommended. Moreover, additional measurements of the noise of a QDM during long periods of time were made in order to understand how the data collection time effects the background noise of the measurements. Measurements showed that there was about $1\mu T$ of background noise after 2 hours and $0.5\mu T$ of background noise after 8 hours. To demonstrate and test the QDM in a real life application, magnetic field measurements of a solenoid sample were carried out. Several MATLAB data analysis programs were created as a result of these investigations, which can be used for conducting additional projects in the near future.

The results of this work demonstrate the principles of operation of the QDM. Future research can build on these results in order to conduct more detailed characterization measurements. Further characterization of the optical system of the QDM would include studying the effect of light polarization on the ODMR spectrum, as well as determining the photon detection rate R in order to calculate volume-normalized sensitivity. The result of these investigation also suggest that conducting future measurements with greater laser power could result in greater magnetic field resolution, and thus should be further investigated. A more detailed description of the behavior of the microwave loop circuit can be made by measuring the scattering parameters of the circuit using a network analyzer. This would enable a more accurate calculation of the power the microwave circuit actually delivers to the sample.

Finally, the work of this investigation could be expanded by conducting a more detailed measurement of the magnetic field of the solenoid, for which an approximate expression for its magnetic field at a given distance can be obtained. Other samples could also be measured. Further validation of the magnetic field data obtained by the QDM by comparison to that obtained from different sources would provide information on how to refine the magnetic field imaging technique.

Bibliography

[1] Levine, E., Turner, M., Kehayias, P., Hart, C., Langellier, N., Trubko, R., Glenn, D., Fu, R. and Walsworth, R. (2019). Principles and techniques of the quantum diamond microscope. Nanophotonics, 8(11), 1945-1973. https://doi.org/10.1515/nanoph-2019-0209

[2] Pham, L. M. (2013) Magentic Field Sensing with Nitrogen-Vacancy Color Centers in Diamond. (PhD Thesis)

[3] McIntyre, David H. (2012) Quantum mechanics: a paradigms approach. Pearson. ISBN 10: 0-321-76579-6 ISBN 13: 978-0-321-76579-6

[4] Griffiths, David J. (2012) Introduction to Electrodynamics. Pearson. ISBN-13: 978-0-321-85656-2 ISBN-10: 0-321-85656-2

[5] Abe, Eisuke et al. (2018) Tutorial: Magnetic resonance with nitrogen-vacancy centers in diamond—microwave engineering, materials science, and magnetometry. Journal of Applied Physics. DOI: 10.1063/1.5011231

[6] Barry John F. et al. (2020) Sensitivity optimization for NV-diamond magnetometry. Reviews of Modern Physics, Volume 92. DOI: 10.1103/RevModPhys.92.015004

[7] Sungkun Hong et al. (2013) Nanoscale magnetometry with NV centers in diamond. Materials Research Society Bulletin, Volume 38. DOI: 10.1557/mrs.2013.23

[8] Takahiro Fukui et al. (2014) Appl. Phys. Express 7 055201

[9] Rabi, I. I. and Zacharias, J. R. and Millman, S. and Kusch, P. (1938) A New Method of Measuring Nuclear Magnetic Moment. Phys. Rev. 53, 318. DOI: https://doi.org/10.1103/PhysRev.53.318

[10] Robledo L., Bernien H., van der Saar T. and Hanson R.(2011) Spin dynamics in the optical cycle of single nitrogen-vacancy centres in diamond. New Journal of Physics 13 (2011) 025013 (11pp) DOI:10.1088/1367-2630/13/2/025013